Dynamic Behavior of a Bluff-Body Diffusion Flame

W. M. Roquemore* and Ronald L. Britton†
Air Force Wright Aeronautical Laboratories, Wright-Patterson Air Force Base, Ohio
and
Sarwan S. Sandhu‡
University of Dayton, Dayton, Ohio

The results of an investigation of the dynamic behavior of a bluff-body stabilized diffusion flame are reported. The dynamic characteristics of flames established by different air and fuel flow rate conditions are investigated using 500 frames/s ciné pictures and two spectrophotometers tuned to the CH emission at 431.5 nm. Each spectrophotometer viewed a 1.8 × 64-mm area of the flame with the long dimension symmetrically located along the diameter. Downstream of the recirculation zone the flame consists of large, discrete "fireballs" or flame turbules separated by axial regions where the flame is not visible. The flame turbules are quasiperiodic with a frequency that decreases as they move downstream. Flame turbule time widths are typically between 1.5 and 12 ms depending on fuel and air flow rates and axial location and their average velocity is approximately equal to the annulus air injection velocity.

Introduction

A RESEARCH combustor has been developed for the purposes of evaluating conventional and advanced laser diagnostic techniques and performing experiments to aid in the evaluation and development of combustion models. During preliminary evaluation of this combustor, high-speed ciné pictures revealed the presence of unsteady flame behavior in the recirculation zone with discrete flame turbules formed further downstream.[1] The purpose of this paper is to describe the characteristics of the flame turbules at different air and fuel flow rate conditions.

A technique that measures the time resolved intensity of optical emissions from free radicals generated by combustion was used to study the time characteristics of the flame turbules. This technique was first employed by Hurle et al.[2] to investigate sound emissions from open premixed turbulent flames. Using an acoustic model that viewed flames as a collection of monopole sound sources, Thomas and Williams[3] developed a relationship between acoustic pressure and optical intensity emitted from a flame. Time-variant pressures calculated by using time-variant C_2 and CH emission intensity data were in quantitative agreement with the pressure values measured by means of a microphone system for frequencies below 1000 Hz. Later, Price et al.[4] and Shivashandara et al.[5] extended the application of the emission technique to the study of noise generation in turbulent gaseous premixed and diffusion flames and liquid-spray combustion. In these studies, care was taken to eliminate continuum emissions from soot because that makes accurate measurements of C_2 emission intensity impossible. Also, the field-of-view of the optical emission technique included the entire flame. Mehta et al.[6] used a slit and lens arrangement to view a small portion of a premixed turbulent flame. Oshima et al.[7] also used spatially resolved C_2 emissions to study sound emission from a burning puff of air-propane gas mixture. This paper extends the technique of using two line-of-sight radical emission measuring systems put forth by Mehta et al.[6] to the study of large-scale, ducted, turbulent, bluff-body diffusion flames.

Presented as Paper 82-0178 at the AIAA 20th Aerospace Sciences Meeting, Orlando, Fla., Jan. 11-14, 1982; submitted Jan. 22, 1982; revision received Nov. 22, 1982. This paper is declared a work of the U.S. Government and therefore is in the public domain.

*Research Scientist, Aero Propulsion Laboratory.
†Electronics Technician, Aero Propulsion Laboratory.
‡Assistant Professor, Department of Chemical Engineering.

Experimental

Combustion Tunnel Facility

A schematic diagram of the research combustor is shown in Fig. 1. The centerbody is 79-cm long and 14 cm in diameter. Gaseous propane fuel is injected at the center of the centerbody face through a 4.8-mm-diam tube and air flows through the annular passage between the outer duct and the centerbody. A 31.8-mm-long square-cell honeycomb flow straightener with a cell size of 4.8 × 4.8 mm and two No. 16 mesh screens are mounted in the annulus. The 25.4-cm-diam duct has 30.5 × 7.6-cm viewing ports that provide both optical and conventional probe access to combusting regions. Additional information about the research combustor is given in Ref. 1.

Optical Emission Measuring System

The optical system is designed to simultaneously measure the time-dependent optical emissions at two axial locations of the flame. The system shown in Fig. 1 consists of two identical ¼-m spectrophotometers, each with an attached fast response photomultiplier tube (PMT) and an external slit and a compound focusing lens. The spectrophotometers, with an estimated bandwidth of 1 nm, were tuned to the (0,0) CH band at 431.5 nm. The outputs of the PMTs were amplified and recorded by either an oscillograph or oscilloscope. The bandpass of the amplifiers was 1000 Hz.

Because the flame turbules in the near-wake region of the centerbody are difficult to resolve by flame emission measurements, it is desirable to optimize the width of the viewing area of the spectrophotometer and the signal strength from the PMT. The optimum condition was obtained using a 0.35-mm-wide slit located 15.24 cm from the surface of the flame. A compound lens, with a focal length of 1.5 cm and located 35.5 cm from the slit, focused the image of the slit onto the entrance plane of the spectrophotometer. The viewing area at the near flame boundary was 1.8 × 64 mm and at the far boundary it was 2.5 × 79 mm.

The two spectrophotometers and the oscillograph recorder were calibrated so they gave equal output voltages for the same input light signal. However, the amplitude of the flame emission is of questionable value due to the presence of soot in different regions of the flame.[2,4] In nonsooting flames, the intensities of the C_2 or CH emissions are assumed to be proportional to their concentrations along the line-of-sight of the viewing area and their concentrations are proportional to

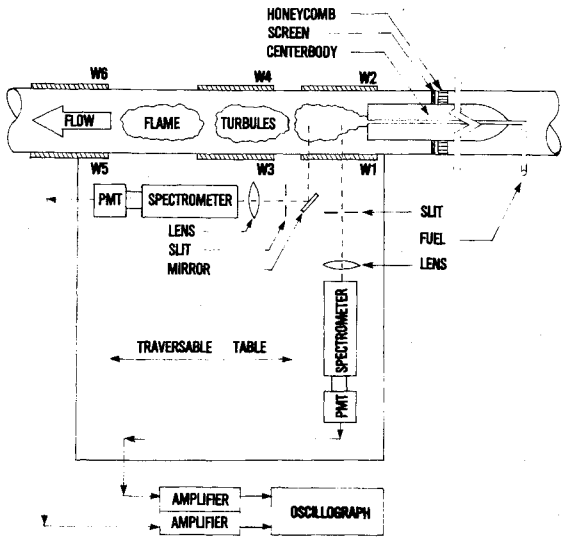

Fig. 1 Schematic of APL combustion tunnel and optical emission system.

the volumetric rate of combustion. A time-averaged emission spectrum shows that the emission bands of C_2, CH, and OH with base bandwidths of approximately 15, 15, and 12 nm, respectively, are superimposed on a continuum background that evidently is caused by the presence of soot. The CH intensity data presented in this paper have not been corrected for the continuum background emissions which varied with test conditions and location in the flame.

A series of experiments was performed to determine if the soot significantly influenced the time characteristics of the flame emissions.[9] For our optical emission detection system, it was found that 1) the time characteristics of the CH plus soot emissions at 431.5 nm and the soot background emission at 448.0 nm were approximately the same when their amplitudes were adjusted to about the same value, 2) the CH emission was about an order of magnitude larger than the amplitude of the background emission, and 3) the time characteristics of the flame emission in the visible spectrum was for practical purposes, independent of wavelength. Hence, the flame emission time characteristics presented in this paper are not believed to be significantly altered by the soot emission.

Test Conditions

Flame turbule characteristics were investigated at different air and fuel flow rates. The combustor was operated at an inlet temperature of 294 K and a barometric pressure of 0.98 atm. The fuel was gaseous propane. Experiments were performed at conditions of 1) varied air flow rates from 1 to 2 kg/s with a fixed fuel flow rate of 13 kg/h and 2) varied fuel flow rates from 4 to 18 kg/h with a fixed air flow rate of 2 kg/s. The Reynolds number for the varied air flow rate experiments ranged from 1.5×10^5 to 3.0×10^5, the average duct velocity and the centerbody diameter were used in the calculations. All of the test conditions were sufficiently removed from the blow-off limits to permit continuous operation of the combustor.

High-Speed Ciné Pictures

A Locam model 51 high-speed tracking camera was used to make 500 frames/s color ciné pictures of the flame. Kodak VNF-7250 film was used and no special processing was required. The camera had a data gate that recorded time to one thousandth of a second on each frame. The framing speed was not sufficient to stop all the flame motion occurring in the recirculation zone. However, it was sufficient to track the motion of large-scale flame structures occurring downstream of the recirculation zone.

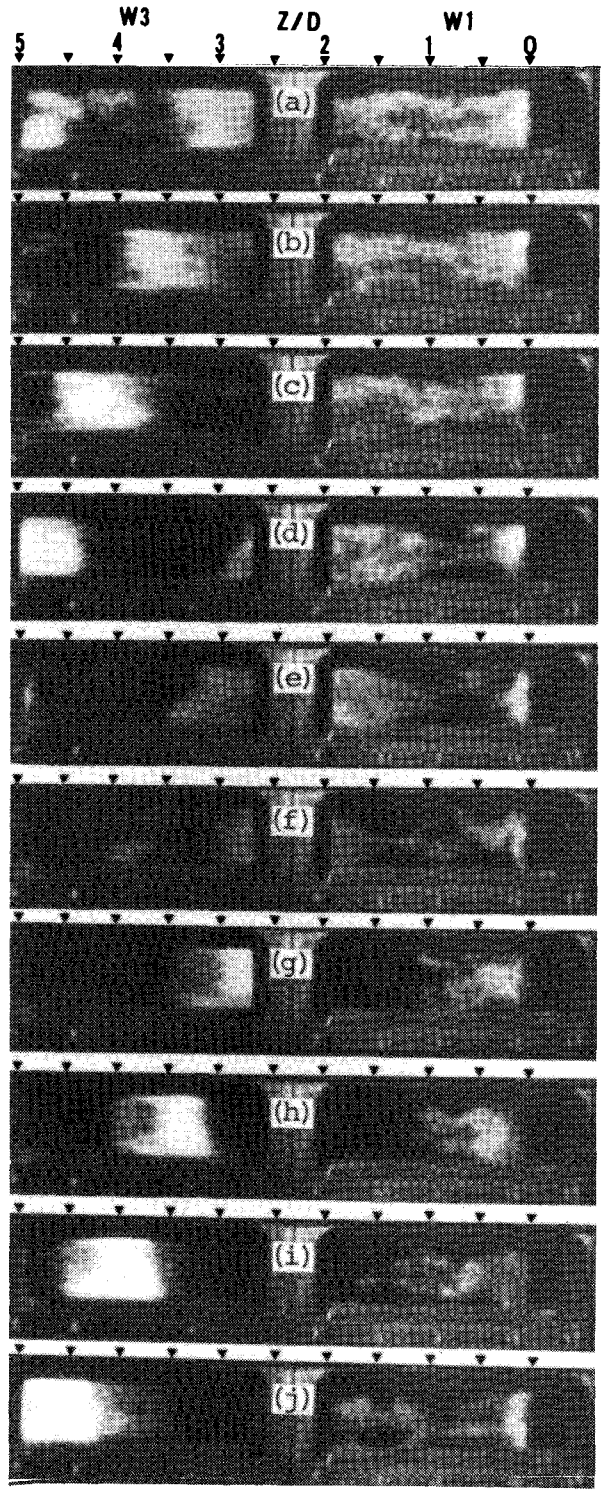

Fig. 2 Sequence of photographs (2 ms apart) showing the formation of a flame turbule for an air flow rate of 2 kg/s and a fuel flow rate of 18 kg/h.

Results

High-Speed Ciné Pictures

High-speed ciné pictures of the flame show a complex, unsteady motion in which discrete islands of flame (flame turbules) are present. The complexity of the motion is most evident in the near-wake recirculation zone of the bluff body where some parts of the flame are moving upstream and other parts are moving downstream and, at the same time, the flame also undergoes some radial and azimuthal motion. Large-scale flame turbules appear to predominate downstream of the recirculation zone. For some air and fuel flow conditions, a flame turbule can be tracked easily over distances of more

than eight centerbody diameters. The large-scale flame turbules are formed quasiperiodically and appear to be the result of the complex motion occurring in the recirculation zone.

The sequence of photographs in Fig. 2 is presented to indicate visually what is meant by a flame turbule; to illustrate size, nonhomogeneous nature, shrinkage and expansion, breakup and coalescence; and to depict the complex flame motion in the recirculation zone. The air flow is from right to left and the Z/D scale is the approximate axial distance measured from the centerbody face (Z) normalized to the centerbody diameter (D). W1 and W3 identify the viewing windows referenced in the schematic in Fig. 1. The recirculation zone is confined to the region viewed through window W1. The centerbody, the bluff end of which extends partway into W1, is axisymmetrically located in the viewing window, but only a little more than half of its diameter is visible due to the height of the window. Examples of flame turbules are given by the luminous region in Fig. 2, photographs c, h, and i at Z/D values between 3.0 and 4.5. These flame turbules are recognized easily because they have well-defined boundaries and are clearly separated from one another.

Time-Resolved CH Emission Records

The velocity, time width, frequency, traceability, and discreteness of flame turbules are evident in the time traces of CH emission intensities shown in Fig. 3. The vertical lines are 10 ms apart and on the original records are separated by 2.0 cm. Figure 3 shows simultaneous recordings at Z/D locations of 3.18 and 4.71 for different air flow rates and for a fuel flow rate of 13 kg/h. The records at $Z/D=3.18$ are believed to be indicative of the characteristics of the turbules as they are formed; whereas, the records at $Z/D=4.71$ give information about the flame turbule decay process. The formation nature of the turbules is very evident in Fig. 3c where, for this low air flow condition, the turbules are not completely formed as noted by the partial establishment of a well-defined zero intensity baseline. As the air flow increases, Figs. 3a and 3b show well-defined zero intensity baselines which indicate completely formed turbules at the upstream measuring station. The records in Fig. 3 also indicate that the time widths of the turbules at the upstream station decrease as the air flow increases. At the downstream station, the number of turbules per unit time (frequency) decreases as the air flow increases.

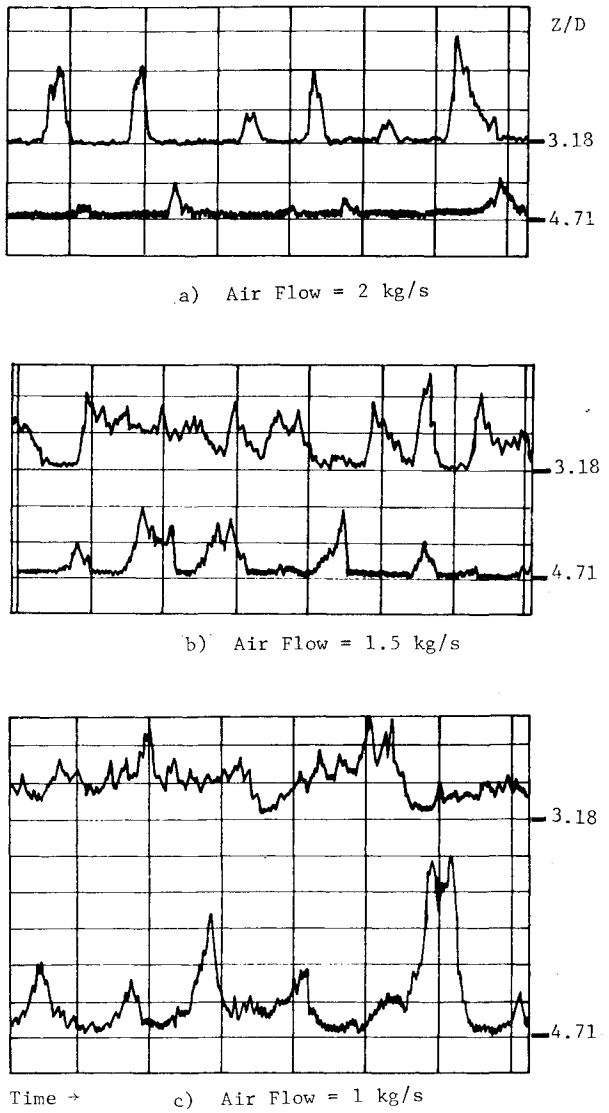

Fig. 3 Simultaneous, time resolve CH emission intensity records at two axial locations for a fixed fuel flow rate of 13 kg/h and varied air flow rates.

Table 1 Analysis of W, F, and time widths as a function of W_A for a fuel flow rate of 13 kg/h and two axial locations[a]

		$Z/D=3.18$				$Z/D=4.71$			
W_A, m/s	W, m/s	F, Hz	t_B, ms	$F\times t_B$	$W\times t_B$, m	F, Hz	t_B, ms	$F\times t_B$	$W\times t_B$, m
23.3	25	-	-	-	-	66	8.3	0.55	0.21
29.1	27	66	10.4	0.69	0.28	65	5.8	0.38	0.16
34.9	32	83	6.1	0.51	0.20	62	4.8	0.30	0.15
40.8	41	84	5.4	0.45	0.22	51	4.2	0.21	0.17
46.6	45	90	4.4	0.40	0.20	44	3.4	0.15	0.15

[a] W = turbule velocity, F = frequency, W_A = annulus velocity. t_B = the time width of the turbule measured at the base of a CH emission peak.

Table 2 Analysis of T_C, W, F, and t_B data as a function of fuel flow (FF) for an air flow of 2 kg/s and a $Z/D=2.86$[a]

FF, kg/h	W, m/s	F, Hz	t_B, ms	$F\times t_B$	T_C, K	$\frac{F\times t_B(\mathrm{FF})}{F\times t_B(18)}$	$\frac{[T_C-T_S](\mathrm{FF})}{[T_C-T_S](18)}$	$W\times t_B$, m
10	50	45	3.8	0.17	728	0.19	0.59	0.19
13	50	104	4.7	0.49	816	0.56	0.73	0.23
16	49	128	5.8	0.74	905	0.84	0.86	0.28
18	49	142	6.2	0.88	994	1.00	1.00	0.30

[a] T_C = centerline temperature, W = turbule velocity, F = frequency, t_B = base time width. T_S = ideal flame temperature for the overall air and fuel flow condition.

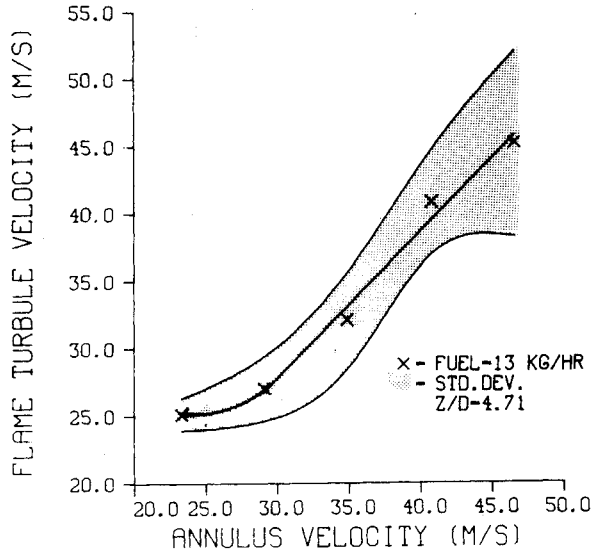

Fig. 4 Average flame turbule velocity as a function of annulus velocity for a fuel flow rate of 13 kg/h.

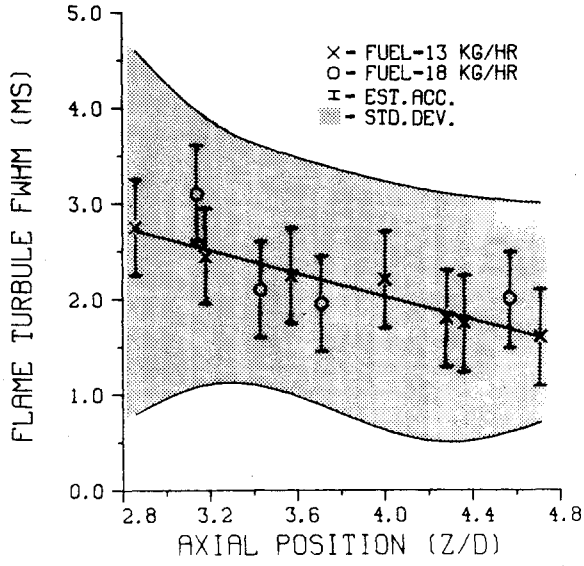

Fig. 6 Average flame turbule time widths (FWHM) as a function of axial location for an air flow rate of 2 kg/s and fuel flow rates of 13 kg/h and 18 kg/h.

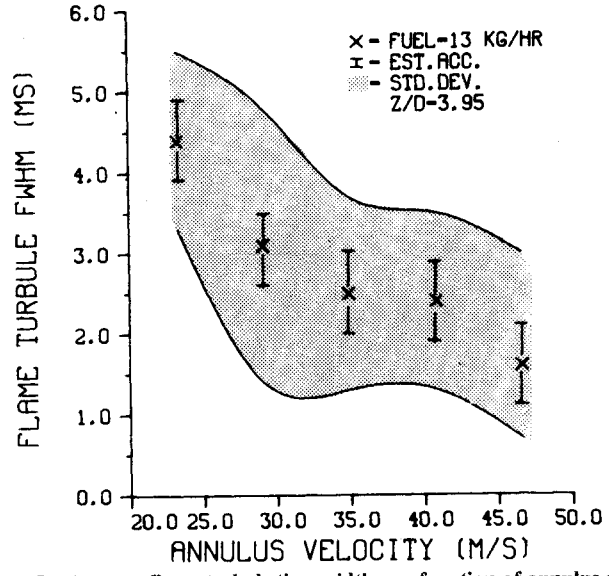

Fig. 5 Average flame turbule time width as a function of annulus air velocity for a fuel flow rate of 13 kg/h at an axial location $Z/D = 4.71$.

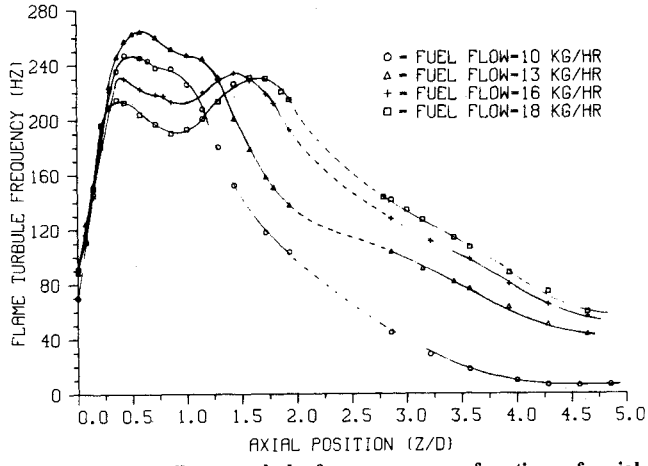

Fig. 7 Average flame turbule frequency as a function of axial position for an air flow rate of 2 kg/s.

Flame Turbule Velocities

The average flame turbule velocities shown in Fig. 4 were determined by measuring the time required for the turbule to travel a distance of 10 cm. The midpoint distance is used as the axial location of the velocity measurement.

Figure 4 shows that, within the experimental error, the average flame turbule velocity is equal to the annulus velocity for all conditions except the lowest annulus velocity condition. For this low-annulus velocity condition, the flame turbule velocity is undoubtedly influenced by the velocity of the injected fuel. Flame turbule velocities were also measured at an air flow rate of 2 kg/s and fuel flow rates of 13 and 18 kg/h at Z/D locations between 1.5 and 3.0. Under these conditions the average velocity of the flame turbules were independent of fuel flow rate and axial location. Their average velocity was about 47 m/s which also corresponds to the annulus air velocity.

Flame Turbule Time Widths

Oscillograph time records such as those shown in Fig. 3 were used to determine the flame turbule time widths. The time widths measured at one-half of the maximum emission intensity are referred to as full-width half-maximum (FWHM) values; whereas, the time widths measured at the baseline are referred to as base-time widths. The time-width data have an unknown bias error due to the integration of the time traces by the 1 kHz bandpass filters and, hence, are used to indicate trends instead of absolute values. In general, the figures contain FWHM values and base-time widths are presented in Tables 1 and 2; however, they both show the same trends for variations in annulus velocity and axial position.

Figure 5 gives the dependence of average flame turbule time width on annulus velocity for a fixed fuel flow rate of 13 kg/h and at a Z/D location of 3.18. The time width is a strong function of annulus velocity and decreases by more than a factor of two with a factor of two increase in annulus velocity. In Fig. 6, there is no apparent dependence of time widths on fuel flow rate at a fixed air flow rate. However, there is a steady decrease in time width with an increase in axial location.

Flame Turbule Frequencies

The data in Fig. 7 are frequency measurements made with a counter coupled to a spectrophotometer. The counter essentially counts the number of voltage pulses in a specified time period with an amplitude greater than a preset trigger

level. For a pulse to be counted, it must extend above and then pass back below the trigger level. The counter is ac coupled to the spectrophotometer so that the trigger level rides on top of a dc background voltage. The trigger level is set so that one or two counts are occasionally recorded in a 10-s sampling period when no flame is present. Setting the trigger level in this way discriminates against the background noise level. However, if the background level varies from day to day, say from spurious light, the trigger level will also vary and repeatable frequency data will not be obtained. To assure that this did not happen, the noise level was checked each test period to make sure that it was below an acceptable level. Also, the flame turbule frequency was measured routinely at a selected combustion condition and at a fixed axial position to assure proper system operation.

It is with some reservation that the frequency data in Fig. 7 are referred to as flame turbule frequencies. Comparisons between the flame turbule frequency measurements made from ciné film, oscilloscope traces, and the counter indicate a reasonable agreement at an axial location downstream of the recirculation zone where the flame turbules are well defined.[9] However, in the recirculation zone, which is confined to Z/D locations between 0.0 and 2.0, the flame turbules are not identified easily from ciné pictures and oscilloscope time records and, thus, no accurate comparisons with the counter results could be made. Because of this, the flame turbule frequency may be a misnomer in this region. The flame turbule frequency connotation is used with the understanding that, in the recirculation zone, it represents a rate of fluctuation of the CH emission intensity and not necessarily a discrete flame turbule that is completely separated from the other flame turbules by nonreacting gases.

Figure 7 shows the appearance of two peaks as the fuel flow rate increases. The axial location of the upstream peak appears to be independent of fuel flow rate and occurs at a Z/D value of 0.4. This suggests that upstream peaks might be determined by the air flow rate. The downstream peak appears to depend on fuel flow rate because the peak becomes more noticeable and moves downstream as the fuel flow is increased. At Z/D locations greater than 2.75, the number of flame turbules per unit time decreases with an increase in axial location. Also, for a fixed axial location, the frequency of the flame turbules increases with an increase in fuel flow rate.

Length and Fraction of Time a Flame Turbule is Present

The axial extent or length of a flame turbule and the fraction of time that a turbule is present at a given axial location can be calculated from the velocity, time width, and frequency data. In a Lagrangian representation such as the ciné pictures in Fig. 2, the flame turbules are observed to have a certain length. Whereas, in the Eulerian view as given by the time records in Fig. 3, the turbules are observed as pulses. The length of a flame turbule can be calculated using the data obtained from the time records. The average flame turbule length is $W \times t_B$ where W is the average axial velocity and t_B is the average base time width of the flame turbules at a given axial location. The base-time width is used instead of the FWHM value because it is believed to give a length that is more comparable to those observed in the ciné pictures. The fraction of time a flame turbule is present at a given axial location is the same as the probability that a turbule is present at this location. It is given by $F \times t_B$ where F is the frequency of the flame turbules at a given axial location.

Tables 1 and 2 give the flame turbule length and the fraction of time flame turbules are present at designated axial locations for different air and fuel flow rates. The data in Table 1 were obtained from oscillograph time records that were obtained simultaneously at the two axial locations. The two axial locations were chosen so that the flame turbules could be characterized shortly after they were formed and after they had a few milliseconds to burn or decay. Review of the ciné pictures shows that the Z/D location where flame

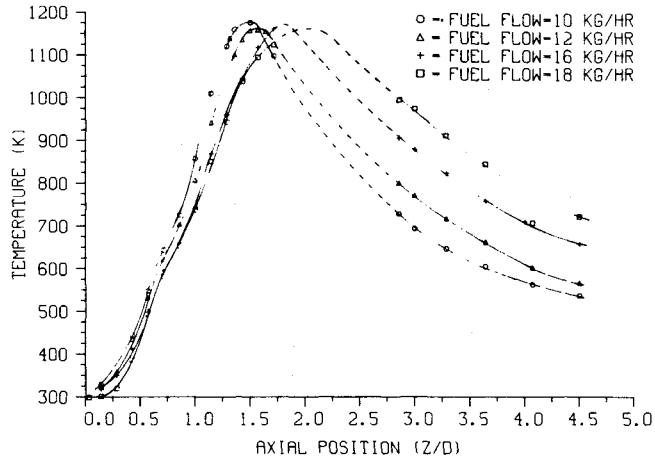

Fig. 8 Average centerline temperature profiles for an air flow of 2 kg/s and different fuel flow rates.

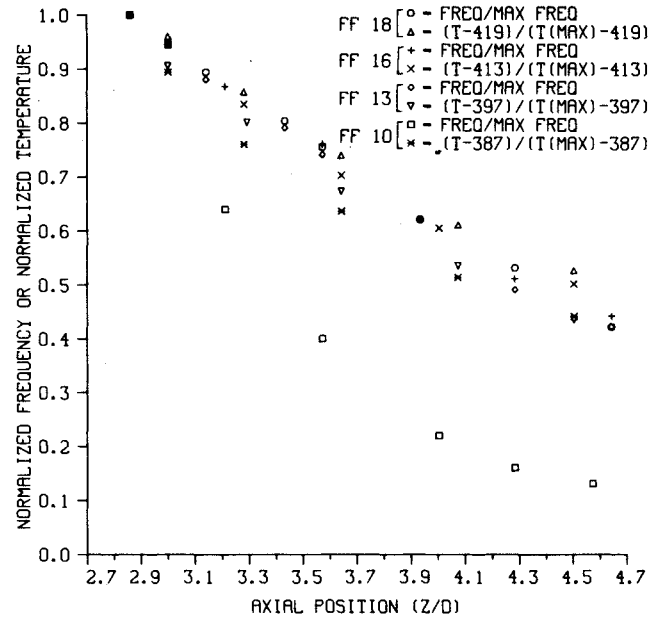

Fig. 9 Normalized flame turbule frequency and centerline temperature profiles for an air flow rate of 2 kg/s and different fuel flow rates.

turbules are formed varies between 1.5 and 3.5 depending on air and fuel flow rates. The data at the axial location of 2.86 in Tables 1 and 2 are believed to be characteristic of newly formed flame turbules.

The data in Table 1 show how the flame turbule characteristics change with variations in air flow rate and the data in Table 2 show the effects of changing the fuel flow rate. It is noted in Table 1 that $F \times t_B$ of the just formed turbules decrease with an increase in air flow rate. This trend is the result of a decrease in t_B since F is noted to increase slightly with an increase in air flow rate. In Table 2 it is noted that $F \times t_B$ increases with an increase in fuel flow rate. This increase is due primarily to the associated increase in flame turbule frequency. These characteristics of the newly formed flame turbules are believed to give important clues about their formation process and will be considered in more detail in the Discussion section.

Time-Averaged Temperatures

Time-averaged data do not always offer the best understanding of turbulent combusting flows and, on occasion, can mask the interesting physics that is taking place. A case in

point is the time-averaged centerline temperature measurements shown in Fig. 8. The similarity of the frequency profiles in Fig. 7 and the temperature profiles are evident, especially for axial locations greater than 2.75. The time-averaged temperatures downstream of the recirculation zone in Fig. 8 are the result of flame turbules and nonluminous regions passing by the thermocouple probe. It seems reasonable that the average temperature should be proportional to the fraction of time that a flame turbule is present. The data in Table 2 supports this idea where the values of $F \times t_B$ for the different fuel flows are normalized to the $F \times t_B$ value at a fuel flow of 18 kg/h. The centerline temperatures (T_C) are normalized to the ideal flame temperature (T_S) that would be obtained by the exhaust gases. In this way, both F and $T_C - T_S$ will be zero at the end of the flame.

Figure 9 contains plots of normalized temperature and frequency data as a function of axial location for an air flow rate of 2 kg/s and for different fuel flow rates. The time-width data are not available for all of these conditions so that $F \times t_B$ values could not be plotted. However, the data in Fig. 6 indicate that the values of t_B should be independent of fuel flow rate so that the normalized values of F should be approximately the same as the normalized values of $F \times t_B$. A very good agreement between the normalized temperature and frequency plots are noted for all but the 10 kg/h fuel flow rate condition. The lack of agreement in this condition might occur because the measurements were made near the end of the flame and appreciable decay of the flame turbules has taken place.

Discussion

The formation of flame turbules downstream of the recirculation zone is the result of dynamic mixing and combustion processes. These dynamic processes are undoubtedly complex and since the flame turbule data are not sufficient to formulate a clear understanding of the processes, any discussions about their formation mechanisms are necessarily incomplete and speculative in nature. Even with these shortcomings, it may prove useful in designing future experiments and formulating new ideas to consider the possible implications of the available data.

It will be useful to first consider a time-averaged description of the flowfield behind the bluff body. The centerbody configuration is thought of as dual jets: an annulus air jet and a central fuel jet. The entrainment of fluid by these jets determines the characteristics of the recirculation zone in the near-wake region of the bluff body separating the jets. Two extreme operating conditions are determined by whether the annulus jet or the fuel jet dominates the flowfield. When the annulus jet dominates, fuel is entrained into the annulus jet establishing a flowfield similar to that shown in Fig. 10a; whereas, with domination by the fuel jet, fuel penetrates the recirculation zone established by the annulus jet and a flowfield similar to that shown in Fig. 10b results. When the annulus jet dominates, the flame is cylindrically shaped with nearly the same diameter as the centerbody and, depending on the air and fuel flow conditions, can extend many diameters downstream. The fuel jet dominated flame has a conical shape similar to that of a free-jet flame. When the air flow rate is high (2 kg/s), the fuel jet can never dominate the flowfield. Instead, at high fuel flow rate conditions, both an annulus jet and a conical fuel jet flame are evident. The velocity data in Ref. 10 indicate that the flowfields for the fuel and air flow rate conditions reported in this paper correspond to that shown in Fig. 10b where most of the fuel penetrates the recirculation zone.

According to the time-averaged view in Fig. 10b, the fuel jet penetrates the recirculation zone continuously. However, this may not be correct when the dynamics of the flowfield is considered. Flame turbules are a mixture of fuel and air in proportions that can maintain combustion. The nonluminous

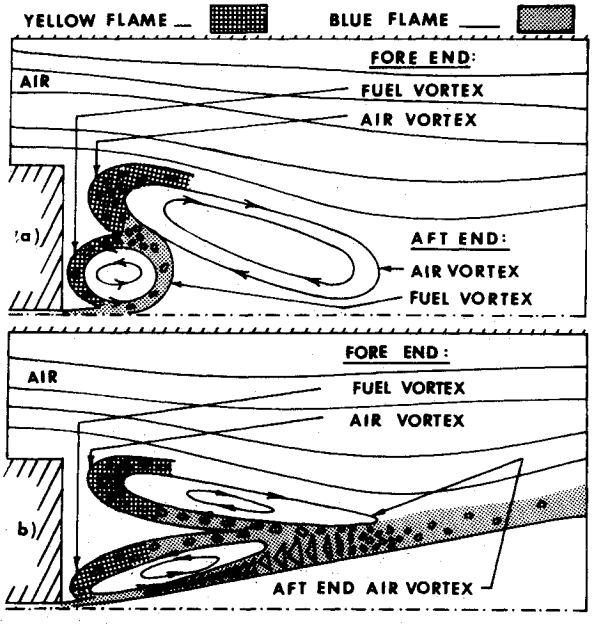

Fig. 10 Illustration of postulated time-averaged flowfields for a high air flow rate and a) a low fuel flow rate and b) a high fuel flow rate.

regions separating flame turbules are where the fuel and air mixture is either too lean or too rich to support combustion. Since the overall combustion efficiency is at least 94% for all of our test conditions, 6% or less of the fuel escapes unburned.[1] From Tables 1 and 2 it can be determined that the nonluminous regions occur 30% or more of the time. These large nonluminous regions must be very fuel lean even if all the unburned fuel is contained in them. For practical purposes, all the fuel escaping the recirculation zone can be assumed to be present in the flame turbules. This indicates that the fuel penetrates the recirculation zone discontinuously. Furthermore, the fraction of time that a turbule is present at an axial location where they are just formed, might also be interpreted as the fraction of time that the fuel penetrates the recirculation zone.

The ciné pictures also indicate that the fuel penetrates the recirculation zone discontinuously or in discrete packets. The formation of a flame turbule is shown in Fig. 2 photographs c-j; however, it is not as evident in the figure as when the ciné pictures are viewed in motion. In photograph c, the flame almost fills window W1. In photograph d, a conically shaped flame, reminiscent of the fuel jet, is apparent. In photographs e, f, and g, the flame appears to move downstream and in photographs h, i, and j, the flame has moved back upstream. The end result is the formation of a turbule, clearly evident in photograph j. This sequence of photographs illustrates that an apparent axial oscillation of the recirculation zone can result in the formation of a flame turbule. This oscillation may be the result of intermittent penetration of the recirculation zone by the fuel jet, as strongly suggested by the conical shape of the flame in Fig. 2d.

The photographs in Fig. 2 also indicate that there may be another way flame turbules are formed. In photographs a and b, a flame turbule results and no axial oscillation has taken place even in pictures prior to photograph a. This flame turbule may be formed as a result of the fuel escaping by means of entrainment into the annulus jet as suggested by the cylindrical shape of the flame in Fig. 2b. However, for our test conditions this probably does not happen very often.

The escaping of fuel and air mixture from the recirculation zone in discrete packets may be the result of large-scale entrainment structures. Breidenthal[11] has performed experiments with both bluff-body and splitter-plate configurations that may give some insight into the dynamic processes leading to the formation of flame turbules. The

experiments were conducted in a two-dimensional water tunnel with reactants A and B separated by a splitter plate or a bluff body. The product formed by the mixing of A and B downstream of the splitter plate was detected by optical absorption in an analogous way that we used the optical CH emissions to detect hydrocarbon reactions. The reaction of A and B was mixing limited and did not result in an appreciable heat release. The product was colored and could be visualized easily by high-speed ciné pictures. The result of this experiment was that the product formed in discrete packets for both splitter-plate and bluff-body flows. Furthermore, the time records of the product were very similar to CH emission time records presented in Fig. 3. Visualization techniques showed that mixing from large-scale structures was responsible for the formation of the discrete packets of product. There are fundamental differences between Breidenthal's experiments and ours, such as the difference in configuration, heat release, and reacting mediums. However, the results appear to be too similar to be coincidental. The results imply that flame turbules might occur because of the interaction of large-scale entrainment structures associated with the annular air jet and the central fuel jet.

As a matter of interest, temperature-time records at the exit plane[12] and inside[13] a gas turbine combustor are sufficiently similar to our CH emission time records and the product time records of Breidenthal's to raise the question about whether large-scale structures might also be present in practical combusting devices. Large-scale structures are also involved in combusting systems with high heat release rates. Ganji and Sawyer[14] and Pitz and Daily[15] have observed that large-scale entrainment structures dominate the flowfield in a two-dimensional rearward facing step (dump) combustor.

Brun et al.[16] suggested that vortex shedding from the face of the bluff body could result in the formation of flame turbules. One can visualize that a toroidal vortex shed from the bluff body could grow, as it moves downstream, to the extent that near the end of the recirculation zone it could interact with the fuel jet. This interaction could momentarily slow down or stop the fuel jet from penetrating the recirculation zone. Such an interaction could lead to the formation of flame turbules, and will be examined in future experiments.

Summary and Conclusions

High-speed ciné pictures and time-resolved measurements of CH emissions were used to study the characteristics of flame turbules formed downstream of the recirculation zone. The velocity frequency and time widths of flame turbules were measured for different air and fuel flow rates and at different axial locations. The results of these measurements can be summarized as follows.

1) The velocity of flame turbules is determined by the annulus air jet injection velocity for almost all air and fuel flow conditions studied.

2) The time width of flame turbules is determined primarily by the annulus air jet and decreases as the air velocity increases for a fixed axial location near where the turbules are formed.

3) The frequency of the flame turbules at an axial location near where they are formed increases with an increase in fuel flow rate.

4) For a fixed air and fuel flow condition, the time width and the frequency decreases as the flame turbules move downstream.

5) Centerline time-averaged temperature measurements downstream of the recirculation zone correlate reasonably well with the fraction of time that a flame turbule is present.

The results are insufficient to establish the flame turbule formation processes but they do lead to speculations about these processes. The formation of flame turbules downstream of the recirculation zone are believed to occur because combustible fuel and air mixtures escape the recirculation zone in discrete packets separated by very lean regions of noncombustible gases. For our test conditions and on a time-averaged basis, the fuel escapes by direct penetration of the recirculation zone by the fuel jet. However, from a dynamic view, the fuel escapes in quasiperiodic bursts that last 1.2-12 ms but occur at a frequency that is sufficiently high to represent an appreciable fraction of the total time. The escape velocity of the fuel appears to be determined primarily by the annulus air velocity. The fraction of the time that fuel does escape (probability of escape) is proportional to the product of the frequency and the time of a burst and varies with air and fuel flow conditions. At a fixed fuel flow rate, the probability of escape decreases with an increase in air flow rate. This decrease results primarily because the actual escape time for each burst decreases substantially with an increase in air flow rate. For a fixed air flow rate, the probability of escape increases with an increase in fuel flow rate. This trend is primarily due to an increase in frequency of the escape process with the actual time of escape being insensitive to the fuel flow rate. Thus, the annulus air jet appears to control the actual time of each burst in which fuel escapes the recirculation zone; whereas, the fuel jet has the most influence on the frequency of the burst. The processes leading to the fuel escaping in discrete packets is undoubtedly complex but may be due to the interaction of shed vortices with the fuel jet.

Acknowledgments

The authors wish to thank Dr. Krishnamurthy, Messrs. R. P. Bradley and Charles Martel, and Dr. A. J. Lightman for their helpful discussions in the course of conducting this research. The authors would also like to express their appreciation to Mr. C. M. Reeves for plotting the graphs, to Mr. Forest Roberts for drawing the illustrations, to Mr. Melvin Russell for operating the combustion tunnel, and to Mr. J. S. Stutrud for his assistance in conducting the thermocouple measurements. The Instrument Development Group at NASA Lewis Research Center designed and fabricated the thermocouple used in this study. A special word of appreciation is extended to Mrs. Bonnie Conover and Mrs. JoAnn Angelos for typing the manuscript.

References

[1] Roquemore, W. M., Bradley, R. P., Stutrud, J. S., Reeves, C. M., and Krishnamurthy, L., "Preliminary Evaluation of a Combustor for Use in Modeling and Diagnostic Development," ASME Pub. 80-GT-93, March 1980.

[2] Hurle, I. R., Price, R. B., Sugden, T. M., and Thomas, A., "Sound Emission from Open Turbulent Premixed Flames," *Proceedings of the Royal Society*, Vol. A303, 1968, pp. 409-427.

[3] Thomas, A. and Williams, G., "Flame Noise: Sound Emission from Spark-Ignited Bubbles of Combustible Gas," *Proceedings of the Royal Society of London*, Vol. A294, 1966, pp. 443-466.

[4] Price, R. B., Hurle, I. R., and Sugden, T. M., "Optical Studies of the Generation of Noise in Turbulent Flames," *Twelfth Symposium (International) on Combustion*, The Combustion Institute, 1968, pp. 1093-1102.

[5] Shivashandara, B. N., Strahle, W. C., and Handley, J. C., "Evaluation of Combustion Noise Scaling Laws by an Optical Technique," *AIAA Journal*, Vol. 13, 1975, pp. 623-627.

[6] Mehta, G. K., Ramachandra, M. K., and Strahle, W. C., "Correlations between Light Emission, Acoustic Emission and Ion Density in Premixed Turbulent Flames," *Eighteenth Symposium (International) on Combustion*, The Combustion Institute, 1981, pp. 1051-1059.

[7] Oshima, J., Kovansznay, L. S. G., and Oshima, Y., "Sound Emission from Burning Puff," *Lecture Notes in Physics, 76, Structure and Mechanisms of Turbulence II, Proceedings*, edited by H. Fiedler, Springer-Verlag, Berlin, 1977.

[8] Yaney, P. P., "Combustion Diagnostics Using Laser Spontaneous Raman Scattering," AFAPL-TR-79-2035, April 1979.

[9] Roquemore, W. M., Britton, R. L., and Sandhu, S. S., "Investigation of the Dynamic Behavior of a Bluff Body Diffusion Flame Using Flame Emissions," AIAA Paper 82-0178, Jan. 1982.

[10] Lightman, A. J. et al., "Velocity Measurements in a Bluff Body Diffusion Flame," AIAA Paper 80-1544, July 1980.

[11] Breidenthal, R., "Structure in Turbulent Mixing Layers and Wakes Using a Chemical Reaction," *Journal of Fluid Mechanics*, Vol. 107, 1981, pp. 1-24.

[12] Dils, R. R., "Dynamic Gas Temperature Measurement in a Gas Turbine Transition Duct Exit," *Journal of Engineering for Power, Transactions of the ASME*, Series A, Vol. 95, No. 3, 1973, p. 265.

[13] Dils, R. R. and Fallansfee, P. S., "Use of Thermocouple for Gas Temperature Measurements in Gas Turbine Combustors," *10th Materials Research Symposium, NBS Special Pub. 561*, Vol. 2, 1979, p. 1027.

[14] Ganji, A. R. and Sawyer, R. F., "Turbulence, Combustion, Pollutant, and Stability Characterization of a Premixed, Step Combustor," NASA Rept. 3230, 1980.

[15] Pitz, R. W. and Daily, J. W., "Experimental Study of Combustion in a Turbulent Free Shear Layer Formed at a Rearward Facing Step," AIAA Paper 81-0106, Jan. 1981.

[16] Brum, R. D., Ikioka, L. M., and Samuelson, G. S., "Axial Flowfield Characteristics of Reacting and Non-Reacting Flows in a Centerbody Configuration," Fall Meeting of the Western States Section of the Combustion Institute, Tempe, Ariz., WSS/CI 81-34, 1981.